BiVO4-TiO2 composite photocatalysts for dye degradation formed using the SILAR method

ARTICLE

$BiVO_4$-TiO_2 composite photocatalysts for dye degradation formed using the SILAR method

Gylen Odling and Neil Robertson*[a]

Abstract: Composite photocatalyst films have been fabricated by depositing $BiVO_4$ upon TiO_2 via a sequential ionic layer adsorption reaction (SILAR) method. The photocatalytic materials were investigated by XRD, TEM, UV-vis diffuse reflectance, ICP-OES, XPS, photoluminescence and Mott-Schottky analyses. SILAR processing was found to deposit monoclinic-scheelite $BiVO_4$ nanoparticles onto the surface, giving successive improvements in the films' visible light harvesting. Electrochemical and valence band XPS studies revealed that the prepared heterojunctions have a type II band structure, with the $BiVO_4$ conduction band and valence band lying cathodically shifted from those of TiO_2. The photocatalytic activity of the films was measured by the decolourisation of the dye rhodamine 6G using $\lambda >$ 400 nm visible light. It was found that 5 SILAR cycles was optimal, with a pseudo 1st order rate constant of 0.004 min^{-1}. As a reference material the same SILAR modification has been made to an inactive wide band gap ZrO_2 film, where the mismatch of conduction and valence band energies disallows charge separation. The photocatalytic activity of the $BiVO_4$-ZrO_2 system was found to be significantly reduced, highlighting the importance of charge separation across the interface. The mechanism of action of the photocatalysts has also been investigated, in particular the effect of self-sensitisation by the model organic dye and the ability of the dye to inject electrons into the photocatalysts conduction band.

Introduction

Contamination of drinking water sources is becoming increasingly problematic in the modern world[1,2]. Photocatalysis has received much attention as a potential method of removing small amounts of highly toxic organic and inorganic compounds from contaminated drinking water in recent years[3–7]. Titanium dioxide (TiO_2) is one of the most popular materials in this field due to its high stability, low toxicity and low cost. However, the activity of TiO_2 is hindered by two factors; a wide band gap which restricts its activity to only UV light, and fast charge recombination leading to few surface reactions occurring. Much work has been devoted to overcoming both these problems including tuning the nanostructure of TiO_2 itself[8–10], doping with non-metals[11–13], metals[14] and combinations of two[15–17] or even more[18] dopants, introduction of plasmonic metal nanoparticles[19,20] and formation of nanocomposites with conductive organic nanomaterials[21,22]. Furthermore, two or more of these methods are often combined to produce high activity photocatalysts[23].

One promising method of providing both visible light harvesting and hindered charge recombination is formation of heterojunctions with narrow band gap inorganic semiconductors such as other metal oxides[24–27] and metal sulphides[28]. Bismuth vanadate ($BiVO_4$) is a cheap, low toxicity replacement for cadmium compounds in the pigment industry and has been investigated as a promising visible-active photocatalyst in its own right[29,30]. Sensitisation of TiO_2 using $BiVO_4$ has been reported to produce photocatalysts with good visible light activity[31,32] by both increasing the absorption into the visible and suppressing charge recombination by providing an interface across which charges are separated.

Herein we describe the formation of immobilised thin film $BiVO_4$-TiO_2 photocatalysts via a sequential ionic layer adsorption reaction (SILAR) method. The immobilisation of photocatalytic material as a film reduces the risk of nanomaterials remaining in the water post purification, a health risk which has generated considerable concern as the use of nanomaterials becomes more prevalent[33,34]. Simplifying the photocatalyst separation process in this way facilitates easy separation and therefore re-use, taking a step toward practical applications. We employ commercially available TiO_2 pastes most commonly used in the fabrication of dye-sensitised solar cells to fabricate films with high surface areas as a base to which SILAR is applied. SILAR is perfectly suited to modification of thin films, and has been applied as a sensitisation technique in solar cells[35,36] where its simplicity, scalability and low costs are advantageous. For the purposes of generating visible-active photocatalysts SILAR is relatively unexplored, and to date has not been used to generate $BiVO_4$. We also describe a new control experiment to examine charge separation in composite nanoparticle films by making comparisons between SILAR modified TiO_2 and ZrO_2 films. As ZrO_2 has a much wider band gap than TiO_2[37] it is both inactive to visible light and disallows charge separation across the $BiVO_4$-ZrO_2 interface. By applying a commercially available ZrO_2 precursor paste designed to be compatible with the TiO_2 used we ensure that the nanoparticle formation and film properties closely resemble that of the TiO_2-$BiVO_4$ film, making the ZrO_2-$BiVO_4$ control a meaningful comparison in all but charge separation.

[a] Prof. N. Robertson
School of Chemistry
University of Edinburgh
Joseph Black Building,
David Brewster Road,
Edinburgh, EH9 3FJ
E-mail: neil.robertson@ed.ac.uk

Supporting information for this article is given via a link at the end of the document.

Results and Discussion

$BiVO_4$ SILAR deposition, structure and morphology

The general SILAR process is detailed in Figure 1. Mesoporous TiO_2 and ZrO_2 films formed using commercially available pastes were chosen as a starting point due to their high surface area, a distinct advantage in catalysis. Upon SILAR cycling, the films became increasingly yellow in colour, corresponding to an increase in the amount of $BiVO_4$ on the surface. Samples will henceforth be named as SILARxN where N = the number of cycles, the SILAR modified ZrO_2 film is termed SILARxN-Z.

The capillary X-ray diffraction trace of the SILARx6 modified sample is shown in Figure 2. Due to the low concentration of $BiVO_4$ present even after 6 SILAR cycles the only peak observed is due to diffraction from the 121 plane (JCPDS card #16-0488), the most intense peak in the monoclinic-scheelite polymorph of $BiVO_4$. A sample of $BiVO_4$ formed by the standard co-precipitation method using the same solutions and heat treatment yielded a pure powder sample of monoclinic-scheelite type $BiVO_4$ (Figure S1), and hence it can be assumed that the SILAR modification of TiO_2 is indeed producing monoclinic-scheelite $BiVO_4$ on the TiO_2 surface. The monoclinic-scheelite structure of $BiVO_4$ has previously been noted to be superior in terms of visible photocatalytic activity to the alternative tetragonal forms owing to lower band gap allowing greater visible light harvesting[38,39]. Similarly when examining a SILARx6-Z control sample (Figure S2), the $BiVO_4$ was found to be very weak, complicated further by the similar diffraction angles of monoclinic and tetragonal ZrO_2[40]. However the same peak that can be assigned to the 121 plane appears upon close examination of the fine area around 30° (Figure S3). Hence it is assumed that the same $BiVO_4$ polymorph is found in both SILARx6 and SILARx6-Z samples indicating that the SILARxN-Z samples provide a good control system to compare with SILARxN.

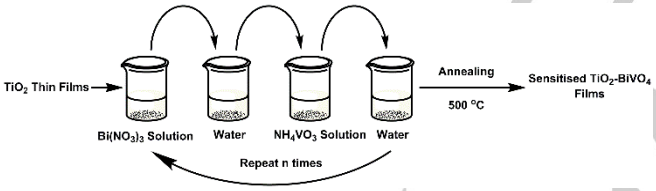

Figure 1. SILAR modification of the prepared films

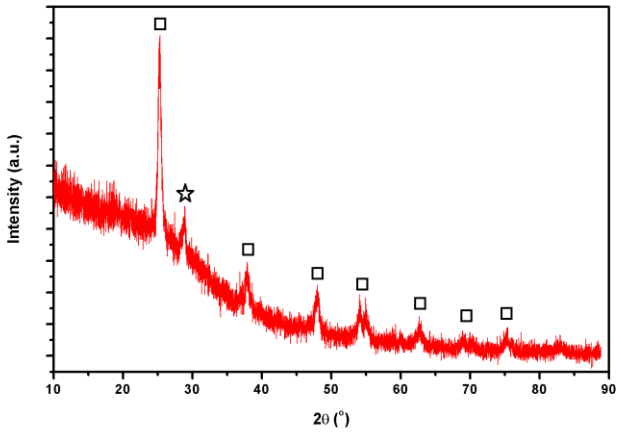

Figure 2. Capillary XRD pattern of SILARx6. (□) anatase TiO_2, (☆) monoclinic-scheelite $BiVO_4$ 121 peak.

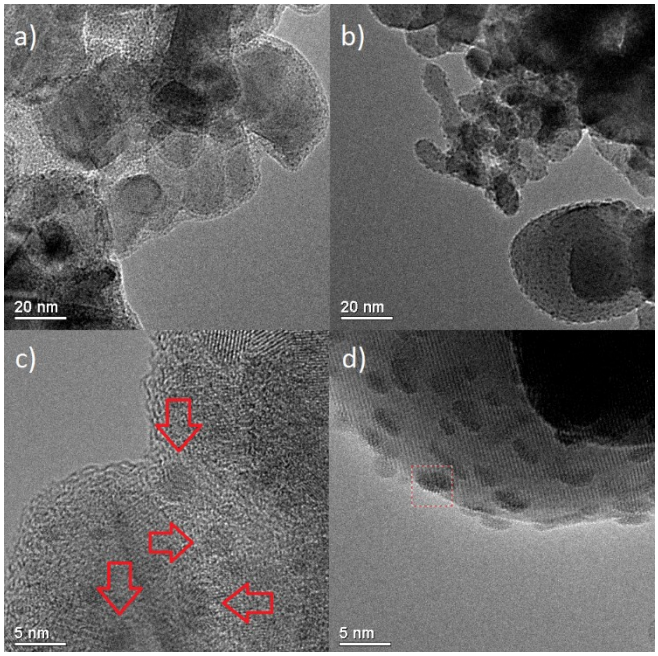

Figure 3. TEM and HR-TEM images of SILARx5 (a and c), and SILARx5-Z (b and d). Red arrows/box highlight $BiVO_4$ nanoparticles on the surface.

Scanning electron microscopy (SEM) images of the films' surface show a porous network of sintered TiO_2/ZrO_2 particles. When comparing a SILAR modified film with a pristine film no observable change in porosity or surface morphology was found (Figure S4), indicating that SILAR is not obstructing the pore structure at all.

To observe the $BiVO_4$ particles higher magnification transmission electron microscope (TEM) images were taken. TEM images of SILARx5 and SILARx5-Z revealed large particles of TiO_2 and ZrO_2 of similar sizes decorated with small nanoparticles of $BiVO_4$ (Figure 3a & 3b). From high resolution TEM images (Figure 3c & 3d) the particles were found to be irregularly shaped with an estimated size of around 5 nm across. The nanoparticle features were observed to be approximately the same in both SILARx5 and SILARx5-Z samples, and therefore differences between the two cannot be ascribed to particle size effects, further establishing the SILARxN-Z system as a meaningful control.

Optical Properties

Incremental increases in the yellow colour intensity was observed upon increasing SILAR cycles, corresponding to the growth of the blue-absorbing $BiVO_4$ on the TiO_2 surface. A shoulder peak corresponding to growth of $BiVO_4$ was observed in the Kubelka-Munk (Figure S5) and corresponding Tauc plots of the SILAR modified material (Figure 4). The band gaps (Eg) of the plain and SILAR modified were determined for each sample from the x-intercept of the Tauc plot according to the Tauc equation‡ and are summarised in table 1.

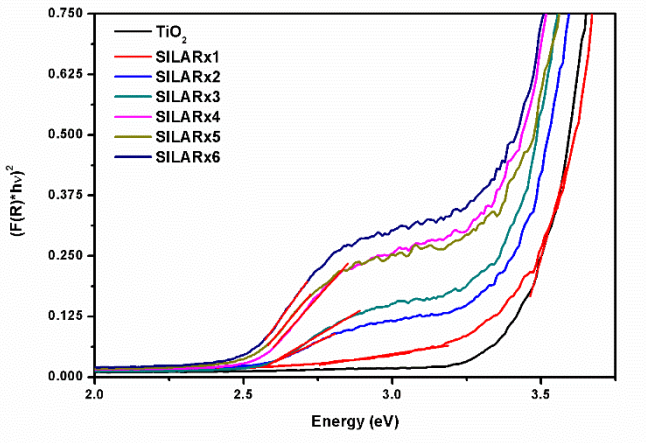

Figure 4. Tauc plots of the $BiVO_4$-TiO_2 composite materials. Linear fits are shown in red.

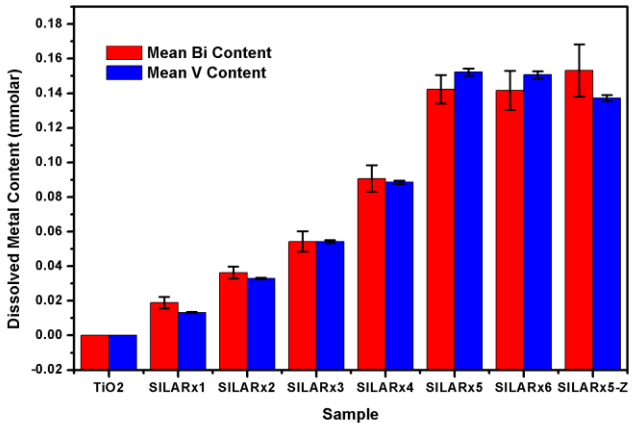

Figure 5. ICP-OES of the dissolved $BiVO_4$

Table 1 Measured Band Gaps

Sample	Band Gap (eV)
TiO_2	3.387
SILARx1	2.482
SILARx2	2.496
SILARx3	2.515
SILARx4	2.510
SILARx5	2.492
SILARx6	2.482

Band gaps were found to be approximately constant across the SILAR modified samples at around 2.5 eV, in accord with the literature[41]. As the number of SILAR cycles increased absorption in the blue region also increased while the bandgap remains largely unchanged, suggesting an increased number of the same sized nanoparticles.

Bulk composition analysis

The bulk composition of the $BiVO_4$ present in the films was determined by dissolving the $BiVO_4$ and performing inductively coupled plasma optical emission spectroscopy (ICP-OES) (Figure 5). Again, increased levels of Bi and V are observed for increased SILAR cycles. Importantly, the levels of Bi and V in SILARx5 and SILARx5-Z are very similar, again verifying the ZrO_2 system as a good control. Additionally, ICP-OES gives further credence to the material analysed being pure $BiVO_4$, as the Bi:V ratio across all samples is within experimental error of 1:1.

X-ray photoelectron spectroscopy

To investigate the chemical speciation of the film surface x-ray photoelectron spectroscopy (XPS) measurements were made. Survey scans (Figure S6) identified the presences of Ti, O, Bi and V. Carbon was also detected, most likely due to adventitious carbon introduced in the processing or measurement, and was used as a reference around the peak at 284.8 eV (Figure S7). High-resolutions XPS scans of the Ti (Figure S8), O (Figure S9), Bi and V peaks were measured, showing an increase in the Bi and V content as the number of SILAR cycles increased (Figure 6). The values obtained for Bi and V are largely consistent with the reported values for Bi^{3+} and V^{5+} in $BiVO_4$[42–45], indicating that no change in oxidation state had occurred during the SILAR processing. Small shifts in the Bi and V peaks to higher binding

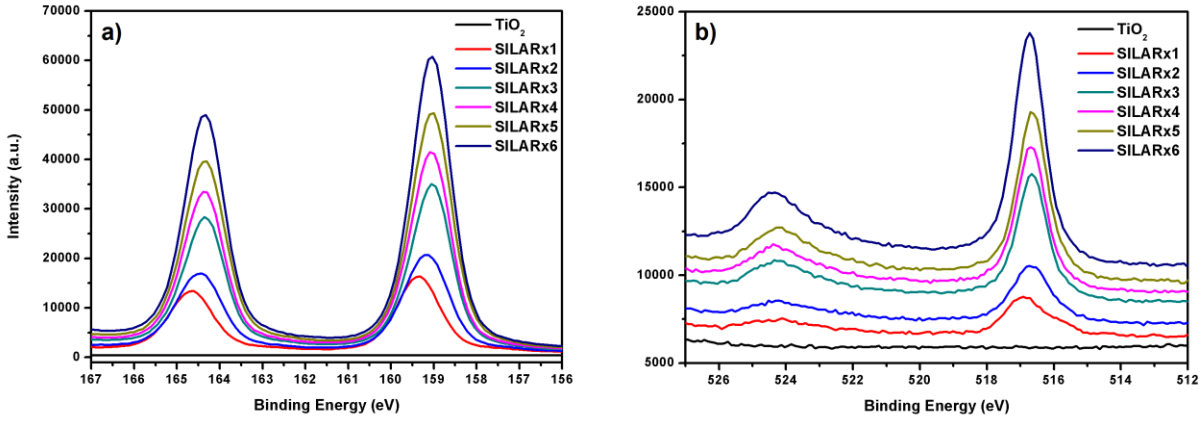

Figure 6. a) Bi^{3+} and b) V^{5+} areas of the films XPS spectra.

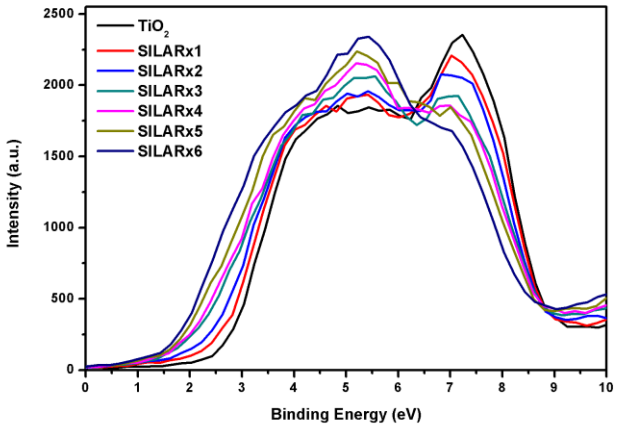

Figure 7. Valence band XPS of the films

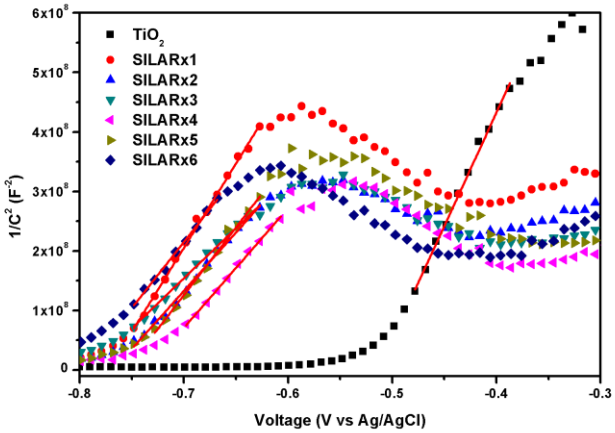

Figure 8. Mott-schottky plots of the films, showing linear region fits in red.

energy in TiO_2-$BiVO_4$ composites compared to the reported values for pure $BiVO_4$ have been previously observed, and rationalised as being due to electron transfer between $BiVO_4$ and TiO_2[32]. To gain insight into the band structure of the prepared composites valence band XPS measurements were carried out (Figure 7). The onset of the valence band was observed to decrease after SILAR processing. From the x-intercepts of the valence band plots the valence band maximum (E_{vb}) was determined (Table 2).

Table 2 Valence band maxima

Sample	Valence Band Maxima (eV)
TiO_2	2.660 ± 0.189
SILARx1	1.858 ± 0.113
SILARx2	1.854 ± 0.078
SILARx3	1.803 ± 0.014
SILARx4	1.818 ± 0.032
SILARx5	1.690 ± 0.021
SILARx6	1.568 ± 0.049

The decrease in E_{vb} can be assigned to photoelectrons emitted from the $BiVO_4$ valence band. Hence there is a ~1 eV driving force for holes to migrate from the TiO_2 to the $BiVO_4$, providing a route for charge separation.

Electrochemical impedance spectroscopy

Mott-Schottky (M-S) analysis is a commonly applied technique used to determine the flat band potential (E_{fb}) of semiconductor materials[45]. The linear portion of the M-S plots (Figure 8) can be extrapolated to the x-intercept to obtain a value for the E_{fb} according to the M-S equation:

$$\frac{1}{C^2} = \frac{2}{e\varepsilon\varepsilon_o N_d}\left(E - E_{fb} - \frac{k_b}{T}\right)$$

Where ε is the dielectric constant of the material, ε_o is the permittivity of a vacuum, N_d describes the charge carrier density, E describes the applied potential, E_{fb} is the flat band potential and k_b/T describes thermal energy, which is considered to be small enough to be safely ignored. The flat band potentials are summarised in table 3.

Table 3 Flat band potentials

Sample	E_{fb} (V vs Ag/AgCl)
TiO_2	-0.507 ± 0.012
SILARx1	-0.771 ± 0.008
SILARx2	-0.771 ± 0.025
SILARx3	-0.797 ± 0.012
SILARx4	-0.746 ± 0.016
SILARx5	-0.753 ± 0.008
SILARx6	-0.792 ± 0.039

Both $BiVO_4$-TiO_2 and TiO_2 exhibited Mott-Schottky plots typical for n-type materials, with a positive gradient in the linear region of the plot, indicating that the majority charge carriers are electrons. The flat band potentials of the TiO_2-$BiVO_4$ heterojunctions are all within experimental error of one another, and are in keeping with the reported values for $BiVO_4$ under similar experimental conditions[45,47–49]. It is known that for n-type materials the flat band is located ~0.1 V anodically from the conduction band minimum[50,51]. Each shows a ~265 mV cathodic shift from the TiO_2, indicating that the SILAR deposited $BiVO_4$ is shifting the flat band upwards in energy by ~265 mV. This indicates that there is a thermodynamic driving force for electron injection, and hence charge separation, across the $BiVO_4$-TiO_2 interface.

Photoluminescence

Photoluminescence (PL) spectroscopy is useful in exploring the extent of charge separation across the $BiVO_4$-TiO_2 interface[31,49]. Emission from $BiVO_4$ has been assigned to recombination of high energy electrons and holes in V3d and O2p orbitals respectively[56,57]. Upon selective excitation of $BiVO_4$ with visible light (400 nm), several bands in the 460-500 nm range were observed in the emission spectrum of both SILARx5 and SILARx5-Z films (Figure 9). The reduction in photoluminescence

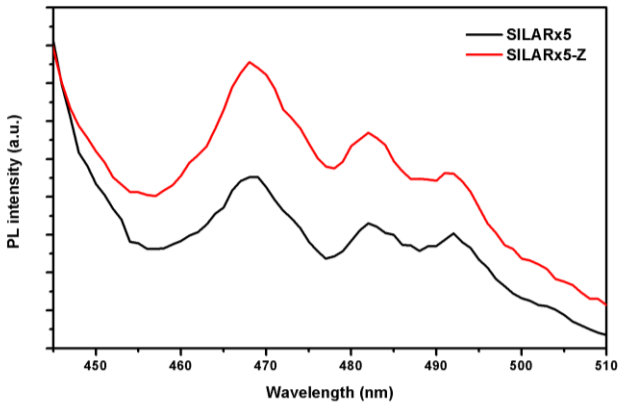

Figure 9. PL spectra of SILARx5 and SILARx5-Z when excited at 400 nm.

from SILARx5-Z to SILARx5 can be rationalised by the energy level matching of $BiVO_4$ with TiO_2 and ZrO_2. As demonstrated the VB and CB edges of $BiVO_4$ lie cathodically shifted from that of TiO_2. This is not the case in the much wider band gap material ZrO_2, where the CB and VB edges lie between those of ZrO_2 and hence charge separation cannot occur between ZrO_2 and $BiVO_4$ and charge recombination prevails (Figure S10). In the case of TiO_2 and $BiVO_4$ the interface allows charge separation and therefore the photoluminescence is lowered.

Photocatalytic tests are often carried out using visible-region absorbing dyes. In this work the dye rhodamine 6G has been used. However, visible irradiation of dyes such as Rh6G causes excitation of both the photocatalyst and the dye. This can cause electron injection from the analyte dye to the photocatalyst conduction band, giving higher rates of degradation in a process known as self-sensitisation.[55] To investigate the ability of Rh6G to charge inject into the conduction bands of $BiVO_4$, TiO_2 and ZrO_2 a series of photoluminescence experiments were carried out. The emission of Rh6G molecules adsorbed onto the surface of the semiconductors was measured upon excitation with 525 nm light (Figure 10). Adsorbed Rh6G on ZrO_2 displays a broad emissive peak around 555 nm, however when adsorbed upon TiO_2, $BiVO_4$-ZrO_2 or $BiVO_4$-ZrO_2 the signal became effectively quenched, indicating that efficient charge separation is occurring which prevents emission (Figure S11). Rh6G is concluded to be able to easily inject excited electrons into the conduction band of TiO_2 and/or $BiVO_4$, therefore demonstrating that the mechanism of photocatalytic action of the composites will be reinforced by self-sensitisation of Rh6G.

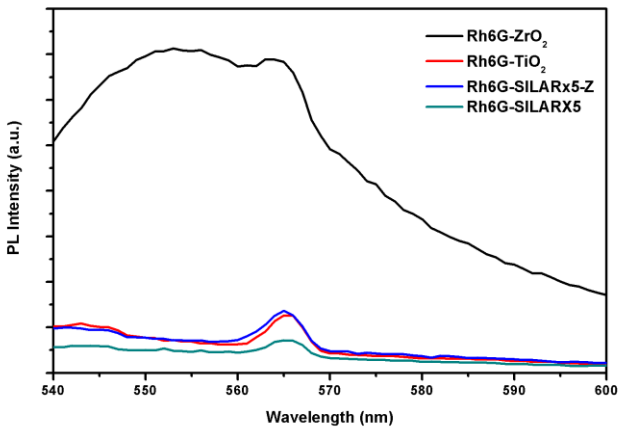

Figure 10. PL spectra of Rh6G adsorbed onto the surface of the semiconductor films.

Band structure

The valence band XPS, Mott-Schottky and photoluminescence analyses have shown that the VB and CB edges of the composites lie cathodically shifted from the plain TiO_2, indicating a band structure known as a type II heterojunction, where electrons move from the conduction band of $BiVO_4$ to the conduction band of TiO_2, and holes vice versa. This structure is in agreement with that described recently by Hu et al[52], Sun et al[53], and Sun et al[31] for $BiVO_4$-TiO_2 heterojunctions.

Photocatalysis

The photocatalytic activity of the composites was assessed using the model organic Rh6G. Glass substrates with the prepared films were submerged in a standard UV-vis cuvette containing 2.5 ml of Rh6G solution and allowed to reach an adsorption/desorption equilibrium for 30 minutes (Figure S12). During this time all films exhibited a small amount of dye adsorption (~10%). The samples were then illuminated from the side using a white LED fitted with a 400 nm long-pass filter (Figure S13). The degradation was then followed using the rhodamine 6G main absorption band at 525 nm. Kinetic parameters of the observed degradation were examined employing the Langmuir-Hinshelwood pseudo-1st order decay model:

$$-\ln\left(\frac{C}{C_0}\right) = k_{app}t$$

Where C/C_0 is the fractional remaining concentration at a particular time, k_{app} is the pseudo 1st order rate constant in min^{-1} and t is time in minutes. Plotting $-\ln(C/C_0)$ against time allows extraction of the pseudo-1st order rate constants easily from the gradient (Figure 11). All the SILAR modified photocatalysts exhibited improved activity over the TiO_2 control, demonstrating the improvement of the SILAR modification. The rate constants of the photocatalysts films and the linear fits R^2 values are summarised in table 4.

Table 4 Pseudo 1st order kinetics of degradation

Sample	Pseudo 1st order rate constants ($x10^{-3}$ min^{-1})	R^2
Photolysis	0.442	0.99717
TiO_2	0.800	0.99803
SILARx5-Z	1.351	0.99918
ZrO_2	0.868	0.99845
SILARx1	1.192	0.99837
SILARx2	2.161	0.98705
SILARx3	2.438	0.99132
SILARx4	3.001	0.98901
SILARx5	4.231	0.99296
SILARx6	3.314	0.99026

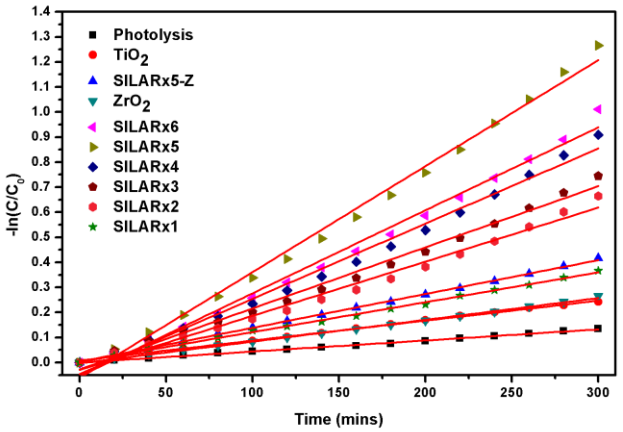

Figure 11. Pseudo first order kinetic plots of the degradation of Rh6G.

It was found that the photodegradation improved in order of the number of SILAR cycles up to a maximum for SILARx5 before decreasing for SILARx6. This optimum number of SILAR cycles is reached despite SILARx6 having marginally better light harvesting than SILARx5. This could be due to there being an optimum coverage of $BiVO_4$ nanoparticles on the TiO_2 surface. A marked improvement is also observed when comparing the photocatalytic activity of the optimum number of SILAR cycles on TiO_2 (SILARx5) to the same number of cycles on ZrO_2 (SILARx5-Z). This highlights the heterojunction effect in the $BiVO_4$-TiO_2 film. The composite performs better than the sum of the individual materials, a difference which can be ascribed to charge separation across the interface.

To eradicate the effects of self-sensitisation, control photocatalytic reactions were run using the colourless organic model pollutants phenol, 4-chlorophenol and catechol. However, no degradation of these organics was observed suggesting that the mechanism of action of the composites does not involve excitation of the $BiVO_4$. This suggests that electron transfer from the Rh6G dye to the semiconductor conduction band is the dominant mechanism in the production of the highly reactive oxygen species that are known for degradation of organic contaminants. Hence the improvement in photocatalytic activity when comparing SILAR modified films is only due to improved charge separation and not visible light sensitisation by the $BiVO_4$ nanoparticles. The mechanism of photocatalytic degradation therefore can be concluded to be as shown (Figure 12).

The photocatalytic films prepared in this work display pseudo 1st order rate constants typically on the lower end of what has been reported in the literature (Table 5). However, it is important to

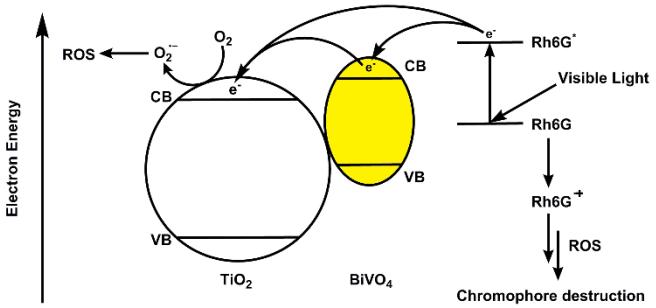

Figure 12. Mechanism of action of the photocatalytic $BiVO_4$-TiO_2 films. VB and CB are valence and conduction bands respectively. ROS refers to a reactive oxygen species such as a hydroxyl radical or hydrogen peroxide.

remember the factors which contribute to photocatalytic activity. Firstly the catalyst loading, which in this work is significantly lower than what is commonly used by others. Secondly the energy and intensity of light used, which can vary significantly from one piece of work to another and in this work was markedly lower than literature comparisons. Thirdly the form of which the catalyst takes, such as a stirred slurry or an immobilised film or wafer, which can dramatically affect mass transfer to the surface. While the degradation of colourless organics has previously been found to be possible using the $BiVO_4$-TiO_2 system in the work detailed in Table 4, it has not been observed in this work despite a band structure that should allow it to occur. It has been established that the activity of the SILAR prepared films under the conditions presented is dominated by self-sensitisation, and it could be that degradation of colourless organics is simply very slow, whereas under similar conditions to those used by others in Table 4 some activity may have been measurable. It is noteworthy that while the films reported here do give lower activities, having the catalyst pre-immobilised is highly advantageous in moving from laboratory interest to real-world applications.

Recyclability testing of SILARx5 showed no loss of activity after five repeat tests of Rh6G photodegradation (Figure 13). In fact, small increases in activity were noted on repeated cycles. This could be due to adsorbed Rh6G molecules retained post washing increasing the self-sensitisation effect.

Conclusions

$BiVO_4$ with the monoclinic-scheelite structure has been deposited upon the TiO_2 surface using the SILAR method. Successive deposition cycles were found to sensitise the TiO_2 to visible light up to the band gap of $BiVO_4$ at ~2.5 eV. The band structure of the

Table 5 Previously reported $BiVO_4$-TiO_2 photocatalysts systems

Analyte	Catalyst Loading & Form	Light Source	k_{app} or % Degradation	Reference
Rhodamine 6G	0.77 ± 0.07 mg film in 2.5 ml	30W White LED >400 nm	0.004 min^{-1}	This Work
Rhodamine B	20 mg powder in 50 ml	6x18W Ne Lamp 400-800 nm	0.026 min^{-1}	Zalfani et al[32]
4-nonylphenol	60 mg powder in 20 ml	300W Xe Lamp >422 nm	0.051 min^{-1}	Li et al[53]
Phenol	100 mg powder in 100 ml	150W Xe Lamp >420 nm	0.005 min^{-1}	Xie et al[52]
Toluene (gaseous)	20 mg wafer in 160 ml reactor	500W Xe Lamp >400 nm	0.006 min^{-1}	Sun et al[31]
Benzene (gaseous)	1.35 g powder in 1.2 ml reactor	500W Xe Lamp 450-900 nm	92% in 8 hours	Hu et al[51]

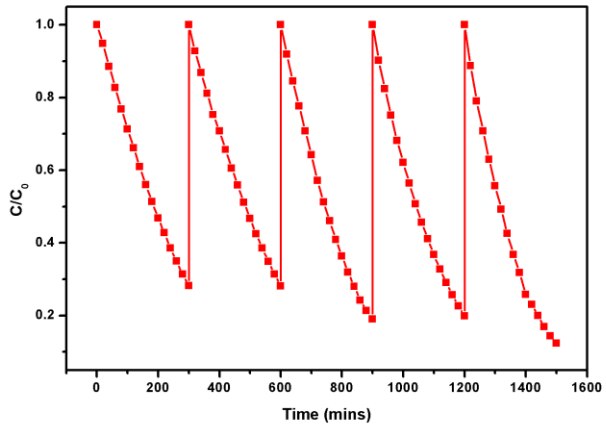

Figure 13. Photocatalytic degradation over five recycles of the SILARx5 film.

composites has been determined by spectroscopic and electrochemical methods to provide a thermodynamic drive for charge separation across the interface as a Type II heterojunction. The photocatalytic efficiency of the prepared films has been investigated by the degradation of the model organic contaminant rhodamine 6G under visible light irradiation. It was found that five SILAR cycles gave optimal photocatalytic activity and good recyclability. The importance of charge separation has been investigated using a new approach in which control films of ZrO_2-$BiVO_4$ were fabricated. These control films were concluded to closely resemble the $BiVO_4$-TiO_2 system in all but charge separation due to mismatching of the conduction and valence band energies, which was found to result in much reduced photocatalytic activity. This provides the first direct photocatalytic evidence between comparable systems, for enhanced performance through interfacial charge separation of a $BiVO_4$-TiO_2 hybrid. The mechanism of action of the composites has been determined to occur via sensitisation by the model organic dye, which has been found to be able to inject charges into the composite conduction band, and hence it can be concluded that charge separation is the main factor in the improvements in activity observed. The work detailed here demonstrates SILAR modified films can be used as a simple, scalable approach to cheap, visible-active photocatalysts with easy separation from solution and good re-usability.

Experimental Section

Chemicals

All reagents were used as received without further purification. Bismuth nitrate pentahydrate (>98%), ammonium metavanadate (99%) and Rhodamine 6G (95%) were purchased from Sigma-Aldrich. The TiO_2 paste was purchased from Dyesol (18NR-T). The FTO glass substrates (TCO30-8) and ZrO_2 paste (Zr-nanoxide ZT/SP) were purchased from Solaronix.

Film preparation

FTO glass substrates were cut into 2cm x 2cm squares before being ultrasonically cleaned in a solution of detergent (Decon 90, ~5% in tap water) for 15 minutes. The substrates were then rinsed with tap water, deionised water and finally ethanol. Titania paste was then doctor bladed in 1 cm x 2 cm strips onto the surface of the FTO before heating to 510 °C in stages on a controlled hotplate to remove the organic templates, leaving a highly porous TiO_2 film. The temperature profile of the heating regime was as follows: 325 °C for 5 minutes, 375 °C for 5 minutes, 425 °C for 5 minutes, 475 °C for 10 minutes, 510 °C for 10 minutes. The heating ramp rate between each stage was 10 °C min^{-1} apart from the final stage where it slowed to 5 °C min^{-1}. The sintered TiO_2 films were then allowed to cool gradually on the hotplate to room temperature. Narrower (0.8 cm x 2 cm) films were also fabricated in the same way for photocatalytic testing and electrochemical characterisation. ZrO_2 films were prepared using the same doctor blading technique, starting from the clean FTO electrodes using a commercially available ZrO_2 paste. After doctor blading the ZrO_2 paste, the films were fired at 400 °C for 30 minutes.

SILAR sensitisation

Aqueous solutions of $Bi(NO_3)_3.5H_2O$ (0.01 M) and NH_4VO_3 (0.01 M) were used as the cation and anion precursors respectively. The as-prepared TiO_2 or ZrO_2 films were submerged first in the $Bi(NO_3)_3$ solution for 30 seconds, then washed with water for 30 seconds to remove any loosely bound material before being submerged in the NH_4VO_3 solution for 30 seconds and finally washed once more with water for 30 seconds. This constitutes one full SILAR cycle, and was repeated 1-6 times to give differing levels of $BiVO_4$ on the substrates. The films were then annealed at 500 °C in a furnace for 1 hour. Samples will henceforth be named as SILARxN where N = the number of cycles, the SILAR modified ZrO_2 film is termed SILARxN-Z. The solutions used for SILAR modification were also used to produce powder $BiVO_4$ samples for XRD analysis.

Characterisation

Films were removed from the substrate with a scalpel and ground before measurement of the XRD traces, TEM images and PL spectra. UV-visible diffuse reflectance of the films was measured using a JASCO V-670 spectrophotometer with an integrating sphere attachment. Photoluminescence (PL) spectroscopy was carried out on a Fluoromax-3 spectrometer at room temperature with an excitation wavelength of 400nm. A fibre optic attachment was used, arranged such that the excitation source was angled at ~45° to the sample and the detector fibre optic at 90°. Photoluminescence quenching on the prepared composites was achieved by leaving the films in a solution of Rhodamine 6G (6 μM) overnight to adsorb onto the surface before measuring the PL spectra using the same setup as described above, but with an excitation wavelength of 525 nm. The sample was backed onto non-emissive black sticky tape for PL measurements. Inductively coupled plasma optical emission spectroscopy (ICP-OES) analysis was carried out on a Perkin Elmer Optima 5300 DV ICP-OES. Solutions for ICP-OES were obtained by dissolving the prepared $BiVO_4$ material in 2 volume% HNO_3. Mott-Schottky analyses were performed using an Autolab PGSTAT30 with FRA software to control a standard three electrode setup. Ag/AgCl reference electrode and Pt wire counter electrode were used, with the film constituting the working electrode, the electrolyte used was 0.05 M Na_2SO_4. XPS scans were carried out using a Kratos Analytical AXIS Nova instrument with monochromated 1486.6 eV Al Kα irradiation. The C 1s peak due to adventitious carbon was used as a calibration peak by alignment to 284.8 eV. X-ray diffraction data were acquired using a STOE STADI P diffractometer operated in capillary Debye-Scherrer mode using monochromated CuKα radiation. Transmission electron microscope (TEM) images were obtained using a Jeol JEM-2011 TEM operated with an accelerating voltage of 200 kV. SEM images were collected using a Carl Zeiss SIGMA HD VP Field Emission SEM, operated in InLens mode with a 10 kV accelerating voltage. In all cases where a result is

accompanied by an error range, the error has been calculated by three measurements on three separately prepared samples.

Photocatalytic testing

Narrow films (0.8 cm x 2 cm) were submerged into a solution of Rhodamine 6G (2.5 ml, 6 µmolar, Absorbance ~ 1) in a borosilicate glass cuvette. The films were stirred in the dark for 30 minutes to establish an adsorption equilibrium, then irradiated with a white LED (7W applied power) fitted with a UV filter (>400 nm, Thorlabs). The decolourisation of Rhodamine 6G was followed by measuring the absorption at 525 nm at regular time intervals using a JASCO V-670 spectrophotometer. Between recyclability tests the photocatalyst films were left stirring in deionised water overnight and then dried for 30 minutes at 130 ºC in an oven before re-use. The spectrum of the LED light source was measured on an Ocean Optics USB2000+ spectrometer.

Acknowledgements

The authors would like to thank the CRITICAT Centre for Doctoral Training (Ph.D. studentship to O.G.; grant code: EP/L016419/1) for financial support. Open data: DOI to be added. X-ray photoelectron spectra were obtained at the National EPSRC XPS Users' Service (NEXUS) at Newcastle University, an EPSRC Mid-Range Facility. TEM images and capillary XRD traces were taken with the assistance of Ross Blackley of the University of St. Andrews. XRD traces were measured by Yuri Andreev of the University of St. Andrews.

Keywords: Photocatalysis • Water Remediation • Semiconductors • Heterojunctions • Charge separation

‡ Tauc Equation: $(F(R_\infty)hv)^2=A(hv - E_g)$ where $F(R_\infty)$ is obtained from the Kubelka-Munk function.

1 World Health Organisation Water Fact Sheet No. 391, *WHO*, 2014.
2 *Water for a sustainable world*, United Nations Educational, Scientific and Cultural Organization, 2015.
3 H. Park, Y. Park, W. Kim, W. Choi, *J. Photochem. Photobiol. C Photochem. Rev.*, **2013**, *15*, 1–20.
4 Y. Sang, H. Liu, A. Umar, *ChemCatChem*, **2015**, *7*, 559–573.
5 Y. Wang, Q. Wang, X. Zhan, F. Wang, M. Safdar, J. He, *Nanoscale*, **2013**, *5*, 8326–39.
6 S. Banerjee, S. C. Pillai, P. Falaras, K. E. O'Shea, J. A. Byrne, D. D. Dionysiou, *J. Phys. Chem. Lett.*, **2014**, *5*, 2543–2554.
7 T. Ochiai and A. Fujishima, *J. Photochem. Photobiol. C Photochem. Rev.*, **2012**, *13*, 247–262.
8 S. Rasalingam, C.-M. Wu, R. T. Koodali, *ACS Appl. Mater. Interfaces*, **2015**, *7*, 4368–4380.
9 Y. Su, Z. Wu, Y. Wu, J. Yu, L. Sun, C. Lin, *J. Mater. Chem. A*, **2015**, *3*, 8537–8544.
10 J. Lu, P. Zhang, A. Li, F. Su, T. Wang, Y. Liu, J. Gong, *Chem. Commun*, **2013**, *49*, 5817–9.
11 Y. Liu, X. Chen, J. Li, C. Burda, *Chemosphere*, **2005**, *61*, 11–18.
12 M. A. Mohamed, W. N. W. Salleh, J. Jaafar, a. F. Ismail, N. A. M. Nor, *Mater. Chem. Phys.*, **2015**, 1–11.
13 C. Sotelo-Vazquez, N. Noor, A. Kafizas, R. Quesada-Cabrera, D. O. Scanlon, A. Taylor, J. R. Durrant, I. P. Parkin, *Chem. Mater.*, **2015**, *27*, 3234–3242.
14 J. Reszczyńska, T. Grzyb, J. W. Sobczak, W. Lisowski, M. Gazda, B. Ohtani, A. Zaleska, *Appl. Catal. B Environ.*, **2015**, *163*, 40–49.
15 M. Antonopoulou, D. Vlastos, I. Konstantinou, *Photochem. Photobiol. Sci.*, **2015**, 520–527.
16 J. Zhao, L. Zhang, W. Xing, K. Lu, *J. Phys. Chem. C*, **2015**, *119*, 7732–7737.
17 Y. Liu, W. Zhou, Y. Liang, W. Cui, P. Wu, *J. Phys. Chem. C*, **2015**, *119*, 11557–11562.
18 N. C. Tolosa, M. C. Lu, H. D. Mendoza, A. P. Rollon, *Appl. Catal. A Gen.*, **2011**, *401*, 233–238.
19 H. Eskandarloo, A. Badiei, M. A. Behnajady, G. Mohammadi Ziarani, *Photochem. Photobiol.*, **2015**, *91*, 797–806.
20 C. T. Dinh, H. Yen, F. Kleitz, T. O. Do, *Angew. Chemie - Int. Ed.*, **2014**, *53*, 6618–6623.
21 H. Li, L. Zhou, L. Wang, Y. Liu, J. Lei, J. Zhang, *Phys. Chem. Chem. Phys.*, **2015**, *17*, 17406–17412.
22 W. Gao, M. Wang, C. Ran, L. Li, *Chem. Commun.*, **2015**, *51*, 1709–1712.
23 M. Wang, J. Han, H. Xiong, R. Guo, Y. Yin, *ACS Appl. Mater. Interfaces*, **2015**, *7*, 6909–6918.
24 S. J. A. Moniz, J. Tang, *ChemCatChem*, **2015**, *7*, 1659–1667.
25 G. Chen, S. Ji, Y. Sang, S. Chang, Y. Wang, P. Hao, J. Claverie, H. Liu and G. Yu, *Nanoscale*, **2015**, *7*, 3117–3125.
26 S. Li, Z. Zhao, Y. Huang, J. Di, Y. Jia, H. Zheng, *J. Mater. Chem. A*, **2015**, *3*, 5467–5473.
27 Z. Lin, P. Liu, J. Yan, G. Yang, *J. Mater. Chem. A*, **2015**, *3*, 14853–14863.
28 Y. Liu, P. Zhang, B. Tian, J. Zhang, *ACS Appl. Mater. Interfaces*, **2015**, *7*, 13849–13858.
29 Y. Kim, D. Shin, W. J. Chang, H. L. Jang, C. W. Lee, H.-E. Lee, K. T. Nam, *Adv. Funct. Mater.*, **2015**, *25*, 2369–2377.
30 R. Munprom, P. A. Salvador, G. S. Rohrer, *J. Mater. Chem. A*, **2015**, *3*, 2370–2377.
31 J. Sun, X. Li, Q. Zhao, M. O. Tadé, S. Liu, *J. Mater. Chem. A*, **2015**, *3*, 21655–21663.
32 M. Zalfani, B. Van Der Schueren, Z.-Y. Hu, J. C. Rooke, R. Bourguiga, M. Wu, Y. Li, G. van Tendeloo, B.-L. Su, *J. Mater. Chem. A*, **2015**, 5165–5171.
33 T. Tong, C. M. Wilke, J. Wu, C. T. T. Binh, J. J. Kelly, J.-F. Gaillard, K. a Gray, *Environ. Sci. Technol.*, **2015**, *49*, 8113–8123.
34 C. Chen, J. M. Unrine, J. D. Judy, R. W. Lewis, J. Guo, D. H. McNear, O. V. Tsyusko, *Environ. Sci. Technol.*, **2015**, *49*, 8759–8768.
35 N. Guijarro, T. Lana-Villarreal, T. Lutz, S. A. Haque, R. Gómez, *J. Phys. Chem. Lett.*, **2012**, *3*, 3367–3372.
36 S. S. Mali, R. S. Devan, Y. R. Ma, C. A. Betty, P. N. Bhosale, R. P. Panmand, B. B. Kale, S. R. Jadkar, P. S. Patil, J. H. Kim, C. K. Hong, *Electrochim. Acta*, **2013**, *90*, 666–672.
37 A. Kudo, Y. Miseki, *Chem. Soc. Rev.*, **2009**, *38*, 253–278.
38 A. Kudo, K. Omori, H. Kato, *J. Am. Chem. Soc.*, **1999**, *121*, 11459–11467.
39 X. Zhang, Z. Ai, F. Jia, L. Zhang, X. Fan, Z. Zou, *Mater. Chem. Phys.*, **2007**, *103*, 162–167.
40 H. Huo, S. Wang, S. Lin, Y. Li, B. Li, Y. Yang, *J. Mater. Chem. A*, **2014**, *2*, 333–338.
41 L. Chen, E. Alarcón-Lladó, M. Hettick, I. D. Sharp, Y. Lin, A. Javey, J. W. Ager, *J Phys Chem C*, **2013**, *117*, 21635-21642.
42 M. D. Rossell, P. Agrawal, A. Borgschulte, C. Hébert, D. Passerone, R. Erni, *Chem. Mater.*, **2015**, *27*, 3593–3600.
43 L. Zhang, D. Chen, X. Jiao, *J. Phys. Chem. B*, **2006**, *110*, 2668–2673.
44 T. S. Sinclair, B. M. Hunter, J. R. Winkler, H. B. Gray, A. M. Müller, *Mater. Horiz.*, **2015**, 22–24.
45 K. P. S. Parmar, H. J. Kang, A. Bist, P. Dua, J. S. Jang and J. S. Lee, *ChemSusChem*, **2012**, *5*, 1926–1934.
46 M. Grätzel, *Nature*, **2001**, *414*, 338–344.
47 H. Ye, J. Lee, J. S. Jang, A. J. Bard, *J. Phys. Chem. C*, **2010**, *114*, 13322–13328.
48 S. J. Hong, S. Lee, J. S. Jang, J. S. Lee, *Energy Environ. Sci.*, **2011**, *4*, 1781.
49 S. Ho-Kimura, S. J. a. Moniz, A. D. Handoko, J. Tang, *J. Mater. Chem. A*, **2014**, *2*, 3948.
50 H. Huang, H. Huang, D. Li, D. Li, Q. Lin, Q. Lin, Y. Shao, Y. Shao, W. Chen, W. Chen, Y. Hu, Y. Hu, Y. Chen, Y. Chen, X. Fu, X. Fu, *J. Phys. Chem. C*, **2009**, *113*, 14264–14269.
51 H. Huang, D. Li, Q. Lin, W. Zhang, Y. Shao, Y. Chen, M. Sun, X. Fu, *Environ. Sci. Technol.*, **2009**, *43*, 4164–4168.
52 Y. Hu, D. Li, Y. Zheng, W. Chen, Y. He, Y. Shao, X. Fu, G. Xiao, *Appl. Catal. B Environ.*, **2011**, *104*, 30–36.
53 M. Xie, X. Fu, L. Jing, P. Luan, Y. Feng, H. Fu, *Adv. Energy Mater.*, **2014**, *4*, n/a–n/a.
54 H. Li, H. Yu, X. Quan, S. Chen, H. Zhao, *Adv. Funct. Mater.*, **2015**, *25*, 3074–3080.
55 M. Rico-Santacruz, Á. E. Sepúlveda, E. Serrano, E. Lalinde, J. R. Berenguer, J. García-Martínez, *J. Mater. Chem. C*, **2014**, *2*, 9497–9504.
56 R. Bajaj, M. Sharma, D. Bahadur, *Dalton Trans.*, **2013**, *42*, 6736.

57 D.-K. Ma, M.-L. Guan, S.-S. Liu, Y.-Q. Zhang, C.-W. Zhang, Y.-X. He and S.-M. Huang, *Dalton Trans.*, **2012**, *41*, 5581.

Entry for the Table of Contents (Please choose one layout)

Layout 1:

ARTICLE

We have use the SILAR technique to prepare a heterojunction photocatalyst based on TiO_2-$BiVO_4$ for water purification. The photocatalyst is formed as a nanocrystalline film ideal for separation and re-use and we use a ZrO_2-$BiVO_4$ control to prove the heterojunction charge separation effect.

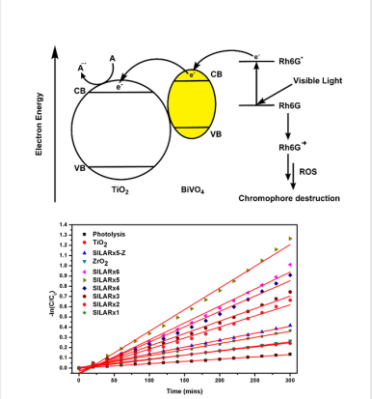

*Gylen Odling, Neil Robertson**

Page No. – Page No.

$BiVO_4$-TiO_2 composite photocatalysts for dye degradation formed using the SILAR method

Layout 2:

ARTICLE

((Insert TOC Graphic here))

*Author(s), Corresponding Author(s)**

Page No. – Page No.

Title

Text for Table of Contents